Decay angular distributions of K^* and D^* vector mesons in pion-nucleon scattering

Sang-Ho Kim,[1,*] Yongseok Oh,[2,1,†] and Alexander I. Titov[3,‡]
[1]*Asia Pacific Center for Theoretical Physics, Pohang, Gyeongbuk 37673, Korea*
[2]*Department of Physics, Kyungpook National University, Daegu 41566, Korea*
[3]*Bogoliubov Laboratory of Theoretical Physics, JINR, Dubna 141980, Russia*
(Received 21 February 2017; published 15 May 2017)

The production mechanisms of open strangeness (K^*) and open charm (D^*) vector mesons in $\pi^- p$ scattering, namely, $\pi^- + p \to K^{*0} + \Lambda$ and $\pi^- + p \to D^{*-} + \Lambda_c^+$, are investigated within the modified quark-gluon string model. To identify the major reaction mechanisms, we consider the subsequent decays of the produced vector mesons into two pseudoscalar mesons, i.e., $K^* \to K + \pi$ and $D^* \to D + \pi$. We found that the decay distributions and density matrix elements are sensitive to the production mechanisms and can be used to disentangle the vector trajectory and pseudoscalar trajectory exchange models. Our results for K^* production are compared with the currently available experimental data and the predictions for D^* production process are presented as well. Our predictions can be tested at the present or planned experimental facilities.

DOI: 10.1103/PhysRevC.95.055206

I. INTRODUCTION

Investigation of open charm and open strangeness production processes is one of the major hadron physics programs at current or planned accelerator facilities that are supposed to provide pion beams [1] or antiproton beams [2].[1] These facilities are expected to produce high-quality beams at energies high enough to produce strange or charm hadrons. Understanding the dynamics of charm and strange quarks is an interesting topic because their mass scale is between the light-quark sector, which is dominated by chiral symmetry, and the heavy-quark sector, where heavy-quark spin symmetry takes a crucial role. Therefore, they are interpolating the two extreme regions and the deviations or corrections to chiral symmetry and heavy-quark symmetry are crucial to understanding the underlying dynamics of the strong interaction.

The heavy mass of the charm quark, in particular, leads to a very rich hadron spectrum with open or hidden charm flavor, which includes exotic states that were not observed in the light-quark sector. Therefore, charm hadron spectroscopy is expected to open a new opportunity for unraveling the strong interaction. Besides, many interesting ideas using charm flavor have been suggested, which include the utilization of charm particles as a probe of nuclear medium at maximum compression, the study of the properties of exotic XYZ mesons, and so on [5,6].

One of the important issues that is not fully resolved at present is the charm and strangeness production mechanisms near threshold in hadron reactions. Because the reaction energy is not high enough to be treated asymptotically, the widely used models for heavy-quark production based on perturbative quantum chromodynamics (pQCD) (see, for example, Refs. [7–9]) are not applicable, and an essential improvement by including high-order corrections is required [10]. Another crucial problem is related to the dynamics of heavy-quark production. In pQCD approaches, charm quarks are produced through gluon fragmentations. To produce charm quarks in peripheral collisions, however, such gluons must have a large momentum ($x \sim 1$), which is much larger than its average magnitude ($x \lesssim 0.2$) inside a nucleon. As a result, this mechanism is strongly suppressed in pQCD and can hardly be the major production mechanism for heavy flavor production at relatively low energies.

Therefore, it is legitimate to rely on the approaches based on a nonperturbative QCD background for describing peripheral reactions. In the present work, we adopt the quark-gluon string model (QGSM) developed by Kaĭdalov and Piskunova in Refs. [11–13], which has been applied for the evaluation of cross sections of the exclusive Λ_c production in pp and $\bar{p}p$ collisions [14–16] and in πp collisions [17–19]. A novel feature of this model is that the invariant amplitude of the binary reaction has a form of the Regge amplitude, where the parameters of effective "Reggeons" are determined by a unitary condition and additivity of intercepts and of inverse slopes of the Regge trajectories.

For such effective Reggeons or effective meson-trajectory exchanges, usually only the vector meson exchange is considered. Since the intercept of the vector meson trajectory is larger than that of the corresponding pseudoscalar trajectory with the same flavor quantum number, the exchange of the pseudoscalar meson trajectory is expected to be suppressed. Therefore, this model would be justified at large center-of-momentum energy squared s and small magnitude of the squared momentum transfer $|t|$. However, to fully understand the production mechanisms, more physical quantities should be examined other than cross sections. In particular, such physical quantities should be sensitive to the production mechanisms whose contribution to cross sections is relatively small. In fact, as we see below, the available data for K^* production suggest

*sangho.kim@apctp.org
†yohphy@knu.ac.kr
‡atitov@theor.jinr.ru

[1]The details of the physics programs using these beams can be found, for example, at the websites of the Japan Proton Accelerator Research Complex (J-PARC) [3] and the Facility for Antiproton and Ion Research in Europe (FAIR) [4].

that the vector meson trajectory exchange model needs to be modified to some extent.

In the present work, we elaborate on the angular distributions of pseudoscalar mesons originated from the decays of vector mesons produced in πN collisions. More specifically, we consider the production of K^* and D^* vector mesons, which decay into $K\pi$ and $D\pi$, respectively. Therefore, the processes under consideration in the present work are the two-step reactions of $\pi N \to K^*\Lambda \to (K\pi)\Lambda$ and $\pi N \to D^*\Lambda_c \to (D\pi)\Lambda_c$, where we specifically work on $\pi^- p$ collisions. In particular, we focus on the angular distributions of K and D mesons produced by these reactions, which bear the information on the production mechanisms of K^* and D^* vector mesons.

This paper is organized as follows. In Sec. II we describe the QGSM, which is used to describe K^* and D^* vector meson productions. All the theoretical tools to investigate the angular distributions of K and D mesons produced by the decays of the corresponding vector mesons are detailed as well. Then, in Sec. III, we show the results on cross sections, spin-density matrix elements, and decay angular distributions of vector mesons produced in $\pi^- p$ collisions. We summarize and conclude in Sec. IV.

II. THE MODEL

The reactions under consideration in the present work are $\pi^- + p \to V + Y \to (P + \pi) + Y$, where Y, V, and P are flavored baryon, vector meson, and pseudoscalar meson, respectively. In the strangeness sector, $Y = \Lambda(1116,1/2^+)$, $V = K^*(892,1^-)$, and $P = K(494,0^-)$, while, in charm sector, $Y = \Lambda_c(2286,1/2^+)$, $V = D^*(2010,1^-)$, and $P = D(1870,0^-)$ [20].

The corresponding cross section for (two-body $\to$ three-body) reactions reads

$$d\sigma = \left(\frac{1}{16\pi\lambda_i}|T_{fi}|^2 dt\right)\left(\frac{k_f d\Omega_f dM_V}{16\pi^3}\right), \tag{1}$$

where T_{fi} is the invariant amplitude for the production process and $\lambda_i \equiv \lambda(M_\pi^2, M_N^2, s)$ is the Källén function defined as $\lambda(x,y,z) \equiv x^2 + y^2 + z^2 - 2xy - 2yz - 2zx$. Here, M_π and M_N stand for the pion mass and the nucleon mass, respectively, and we use M_V for the vector meson mass. The Mandelstam variables for the production process are defined as $s = (p_\pi + p_p)^2 = (p_V + p_Y)^2$ and $t = (p_p - p_Y)^2 = (p_\pi - p_V)^2$, where p_π, p_p, p_V, and p_Y are the four momenta of the pion, the proton, the produced (virtual) vector meson, and the hyperon, respectively. The solid angle and the magnitude of the three-momentum of the outgoing pseudoscalar meson in the rest frame of the vector meson are represented by Ω_f and k_f, respectively. The averaging over the initial spin states and the sum over the final spin states are understood as well.

The invariant amplitude can be expressed as

$$T_{fi} = \mathcal{A}_{m_f,\lambda_V;m_i}\frac{1}{p_V^2 - M_0^2 + iM_0\Gamma_{\rm tot}}\mathcal{D}_{\lambda_V}(\Omega_f), \tag{2}$$

where m_i and m_f denote the spin projections of incoming and outgoing baryons, respectively, and λ_V represents the spin projection of the produced virtual vector meson. M_0 and $\Gamma_{\rm tot}$ are the pole mass and the total decay width of the produced vector meson, respectively. The amplitudes of the $\pi^- + p \to V + Y$ and $V \to P + \pi$ reactions are denoted by $\mathcal{A}$ and $\mathcal{D}$, respectively. The decay process of the vector meson is considered in its rest frame. In this case, the amplitude of the vector meson decay into two pseudoscalar mesons has the simple form of

$$\mathcal{D}_\lambda = 2c\sqrt{\frac{4\pi}{3}}Y_{1\lambda}(\Omega_f), \tag{3}$$

where the constant c is related to the $V \to P + \pi$ decay width Γ_f as

$$c^2 = \frac{6\pi M_V^2\Gamma_f}{k_f}, \tag{4}$$

with k_f being the magnitude of the three-momentum of the final-state particles in the rest frame of the vector meson. Integration of $d\sigma$ in Eq. (1) over dM_V and $d\Omega_f$ leads to the well-known result for the corresponding unpolarized cross section,

$$\frac{d\sigma}{dt} = \frac{\rm Br}{16\pi\lambda_i}|\mathcal{A}_{fi}|^2, \tag{5}$$

with ${\rm Br} = \Gamma_f/\Gamma_{\rm tot}$ when $\Gamma_{\rm tot} \ll M_V$.

Recent studies of strangeness and charm production at a few dozen GeV show that this cross section can be successfully evaluated in the framework of the QGSM suggested by Kaidalov [11,12] and later developed and refined in a number of theoretical works developed, for example, in Refs. [13–19]. The QGSM is based on the planar quark diagram decomposition and unitary conditions [12], and it allows one to represent the amplitude of the binary $a + b \to c + d$ reaction in terms of an effective Regge amplitude, where the effective trajectory $\alpha_{\mathcal{R}}(t)$ and the energy scale parameter $s_{ab;cd}$ are determined by the well-established parameters of the elastic $a + b \to a + b$ and $c + d \to c + d$ reactions using the so-called planar diagram decomposition. An example of the planar diagram decomposition is depicted in Fig. 1 for the reaction of $\pi^- + p \to D^{*-} + \Lambda_c^+$, where it is assumed that the amplitude is dominated by the effective D^* trajectory with parameters completely determined by the nonlinear ρ and J/ψ meson trajectories as found from the meson spectroscopy studies [12,21,22]. Similarly, one can write the planar diagram decomposition for the $K^*\Lambda$ production with substitution of the J/ψ trajectory by the ϕ meson trajectory. The details can be found in Ref. [15].

Diagrammatic representations of the effective $\pi^- + p \to K^{*0} + \Lambda$ and $\pi^- + p \to D^{*-} + \Lambda_c^+$ reactions are shown in

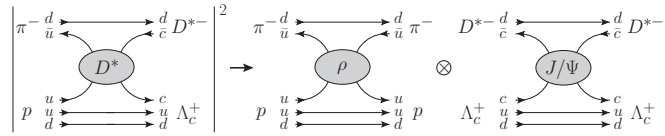

FIG. 1. Planar diagram decomposition for the reaction of $\pi^- + p \to D^{*-} + \Lambda_c^+$.

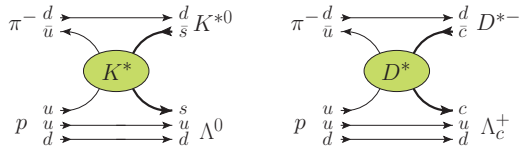

FIG. 2. Diagrammatic representation of the effective $\pi^- + p \to K^{*0} + \Lambda$ and $\pi^- + p \to D^{*-} + \Lambda_c^+$ reactions.

Fig. 2. The corresponding spin-independent amplitudes read

$$\mathcal{A}^V_{fi} = g_0^2 \frac{s}{\bar{s}} \Gamma\big(1 - \alpha^V_{\mathcal{R}}(t)\big)\left(\frac{s}{s^V_{0\mathcal{R}}}\right)^{\alpha^V_{\mathcal{R}}(t)-1}, \tag{6}$$

with $\alpha^V_{\mathcal{R}_{p\Lambda}}(t) = 0.414 + 0.707\,t$, $s^V_{0\mathcal{R}_{p\Lambda}} = 1.66\ \mathrm{GeV}^2$, and $\bar{s}_{p\Lambda} = 1\ \mathrm{GeV}^2$ for $\pi^- + p \to K^{*0} + \Lambda$, and $\alpha^V_{\mathcal{R}_{p\Lambda_c}}(t) = -1.02 + 0.467\,t$, $s^V_{0\mathcal{R}_{p\Lambda_c}} = 4.75\ \mathrm{GeV}^2$, and $\bar{s}_{p\Lambda_c} = 1\ \mathrm{GeV}^2$ for $\pi^- + p \to D^{*-} + \Lambda_c^+$. The trajectories of ρ, ϕ, and J/ψ, as well as the energy-scale parameters $s^V_{0\mathcal{R}}$, are determined following the prescription described in Ref. [15]. The residual factor g_0 is determined in the next section by comparison with the available experimental data for the $\pi^- + p \to K^{*0} + \Lambda$ reaction, which leads to $g_0^2/4\pi \simeq 0.796$.

Because the angular distributions of pseudoscalar mesons produced through the decays of $K^* \to K + \pi$ and $D^* \to D + \pi$ strongly depend on the spin of the participating particles, the spin structure of the reaction amplitudes of Eq. (6) should be specified. This, in fact, is the key component that can distinguish different production mechanisms. It can be done by "dressing" the spin-independent amplitude by the spin factor S_{fi} that carries the symmetry of the exchanged Reggeon [15], i.e.,

$$\mathcal{A}_{fi} \to \mathcal{A}_{m_f,\lambda_V;m_i} = \mathcal{A}_{fi}\,\frac{1}{\mathcal{N}}\,S_{m_f,\lambda_V;m_i}, \tag{7}$$

with the normalization factor

$$\mathcal{N}^2 = \sum_{m_f,m_i,\lambda_V} \big|S_{m_f,\lambda_V;m_i}\big|^2. \tag{8}$$

The K^*-meson coupling in the spin factor S_{fi} reads

$$S_{m_f,\lambda_V;m_i} = \epsilon^{\mu\nu\alpha\beta} q_\mu p_{V\alpha} \varepsilon^*_\beta(\lambda_V) \times \bar{u}_{m_f}(\Lambda) \times \left[(1 + \kappa_{K^*p\Lambda})\gamma_\nu - \kappa_{K^*p\Lambda}\frac{(p_p + p_\Lambda)_\nu}{M_p + M_\Lambda}\right] u_{m_i}(p), \tag{9}$$

where $q = p_V - p_\pi = p_p - p_\Lambda$ is the momentum transfer and $\kappa_{K^*p\Lambda} = 2.79$ is the tensor coupling constant obtained from the average value of the Nijmegen soft-core potential [23,24]. The Dirac spinors of the initial baryon and the final baryon are denoted by u_{m_i} and u_{m_f}, respectively, and $\varepsilon(\lambda_V)$ is the polarization vector of the produced vector meson. Generalization to the case of charm production may be achieved by the substitutions $M_\Lambda \to M_{\Lambda_c}$, $M_{K^*} \to M_{D^*}$, and so on. Because of the lack of information, we assume $\kappa_{K^*p\Lambda} = \kappa_{D^*p\Lambda_c}$ as in Ref. [25]. The normalization factor $\mathcal{N}$ in Eq. (7) is introduced to compensate for the artificial s and t dependence generated by S_{fi}.

The differential cross section is then written as

$$\frac{d\sigma}{dt\,d\Omega_f} = \frac{d\sigma}{dt}\,W(\Omega_f), \tag{10}$$

where

$$W(\Omega_f) = \sum_{m_i,m_f,\lambda_V,\lambda'_V} \mathcal{M}_{m_f,\lambda_V;m_i}\mathcal{M}^*_{m_f,\lambda'_V;m_i} \times Y_{1\lambda_V}(\Omega_f)\,Y^*_{1\lambda'_V}(\Omega_f), \tag{11}$$

with

$$\mathcal{M}_{m_f,\lambda_V;m_i} = \frac{1}{\mathcal{N}}\,S_{m_f,\lambda_V;m_i}. \tag{12}$$

For definiteness with the isospin quantum number we consider $K^{*0} \to K^+\pi^-$ and $D^{*-} \to D^-\pi^0$ decays. As is well known, since the decay angular distribution of outgoing K^+ is analyzed in the virtual vector meson's rest frame, there is an ambiguity in choosing the quantization axis. One may choose the quantization axis antiparallel to the outgoing hyperon Y in the center-of-momentum frame of the production process or the quantization axis may be defined to be parallel to the incoming pion, i.e., the initial beam direction. Following the convention of Ref. [26], the former is called the s frame and the latter the t frame.[2]

The decay probabilities are expressed in terms of the spin-density matrix elements $\rho_{\lambda\lambda'}$, where λ_V is abbreviated as λ, which are determined by the amplitudes of Eq. (12). Depending on the polarization state of the initial and final states, we are interested in the following two cases:

(i) the unpolarized case, where the spin-density matrix is given by

$$\rho^0_{\lambda\lambda'} = \sum_{m_i=\pm\frac{1}{2},\,m_f=\pm\frac{1}{2}} \mathcal{M}_{m_f,\lambda;m_i}\,\mathcal{M}^*_{m_f,\lambda';m_i}, \tag{13}$$

(ii) the recoil polarization case, when the spin of the outgoing hyperon (Λ) is determined by their decay distribution using that it is self-analyzing. Then, depending on the spin state of the hyperon, we have two kinds of spin-density matrices defined as

$$\rho^\pm_{\lambda\lambda'} = \sum_{m_i=\pm\frac{1}{2}} \mathcal{M}_{m_f,\lambda;m_i}\,\mathcal{M}^*_{m_f,\lambda';m_i}. \tag{14}$$

Here, ρ^+ and ρ^- correspond to the cases when the spin or helicity of the produced hyperon is $m_f = +\frac{1}{2}$ and $-\frac{1}{2}$, respectively.

Denoting the polar and the azimuthal angles of the outgoing pseudoscalar K (or D) mesons by Θ and Φ, respectively, the decay angular distributions can be expressed in terms of the spin-density matrix elements as

$$W^0(\Omega_f) = \frac{3}{4\pi}\big[\rho^0_{00}\cos^2\Theta + \rho^0_{11}\sin^2\Theta - \rho^0_{1-1}\sin^2\Theta\cos 2\Phi - \sqrt{2}\,\mathrm{Re}\big(\rho^0_{10}\big)\sin 2\Theta\cos\Phi\big], \tag{15}$$

[2]In the case of vector meson photoproduction, the former is called the helicity frame, while the latter corresponds to the Gottfried-Jackson frame [27].

for the unpolarized case, and

$$W^{\pm}(\Omega_f) = \frac{3}{4\pi}\Big[\rho^{\pm}_{00}\cos^2\Theta + \frac{1}{2}(\rho^{\pm}_{11}+\rho^{\pm}_{-1-1})\sin^2\Theta - \rho^{\pm}_{1-1}\sin^2\Theta\cos 2\Phi - \frac{1}{\sqrt{2}}\mathrm{Re}(\rho^{\pm}_{10}-\rho^{\pm}_{-10})\sin 2\Theta\cos\Phi\Big], \quad (16)$$

for the case of recoil polarization. Here, we made use of the following Hermitian conditions: $\rho_{-11} = \rho_{1-1}$, $\rho_{01} = \rho_{10}$, and $\rho_{0-1} = \rho_{-10}$. In addition, for unpolarized reactions, we also have the sum rule $\rho^0_{00} + \rho^0_{11} + \rho^0_{-1-1} = 1$ and the symmetry conditions $\rho^0_{11} = \rho^0_{-1-1}$ and $\rho^0_{01} = -\rho^0_{0-1}$. In the case of recoil polarization, however, these additional relations do not hold.

As was mentioned earlier, the purpose of the present work is to test the validity of the dominance of vector meson trajectory exchange. This assumption is based on the observation that the intercept of the K^* (D^*) vector meson, for instance, is larger than that of the corresponding pseudoscalar K (D) meson trajectory [21]. However, other mechanisms cannot be excluded, and the contribution from such mechanisms should be verified by physical quantities related to the spin structure of the production mechanisms. In fact, as we see later, the available data for density matrix elements suggest that there exist contributions from mechanisms other than vector trajectory exchange. Therefore, in addition to vector trajectory exchanges, we consider the exchanges of effective pseudoscalar K and D trajectories. In this case, the spin-independent amplitude reads

$$\mathcal{A}^{\mathrm{PS}}_{fi} \simeq g_0^2\,\Gamma\big(-\alpha^{\mathrm{PS}}_{\mathcal{R}}(t)\big)\left(\frac{s}{s^{\mathrm{PS}}_{0\mathcal{R}}}\right)^{\alpha^{\mathrm{PS}}_{\mathcal{R}}(t)}, \quad (17)$$

with $\alpha^{\mathrm{PS}}_{\mathcal{R}_{p\Lambda}}(t) = -0.151 + 0.617\,t$ and $\alpha^{\mathrm{PS}}_{\mathcal{R}_{p\Lambda_c}}(t) = -1.611 + 0.439\,t$ [22]. The energy scale parameters determined by the flavor content of the vertices are assumed to be the same as those in the vector meson exchange case so that $s^{\mathrm{PS}}_{0\mathcal{R}_{p\Lambda}} = s^{V}_{0\mathcal{R}_{p\Lambda}}$ and $s^{\mathrm{PS}}_{0\mathcal{R}_{p\Lambda_c}} = s^{V}_{0\mathcal{R}_{p\Lambda_c}}$. The spin factor S_{fi} now reads

$$S^{\mathrm{PS}}_{m_f,\lambda_V;m_i} = \varepsilon^*_\mu(\lambda_V)\,q^\mu\,\bar{u}_{m_f}(\Lambda)\gamma_5 u_{m_i}(p). \quad (18)$$

III. RESULTS AND DISCUSSION

In this section, we present numerical results on differential cross sections, spin-density matrix elements, and decay angular distributions of K and D mesons in πN scattering.

A. Unpolarized cross sections

By collecting all information, the unpolarized differential cross sections of the $\pi^- + p \to K^{*0} + \Lambda$ and $\pi^- + p \to D^{*-} + \Lambda_c$ reactions for the vector (V) and pseudoscalar (PS) effective Reggeon exchanges are written as

$$\frac{d\sigma^{(V)}}{dt} = \frac{\pi}{\lambda_i}\left(\frac{s}{\bar{s}}\right)^2\left[\frac{\big(g^V_0\big)^2}{4\pi}\right]^2[\Gamma(1-\alpha^V(t))]^2 \times\left(\frac{s}{s_{0\mathcal{R}^V}}\right)^{2(\alpha^V(t)-1)},$$

$$\frac{d\sigma^{(\mathrm{PS})}}{dt} = \frac{\pi}{\lambda_i}\left[\frac{\big(g^{\mathrm{PS}}_0\big)^2}{4\pi}\right]^2[\Gamma(-\alpha^{\mathrm{PS}}(t))]^2\left(\frac{s}{s_{0\mathcal{R}^{\mathrm{PS}}}}\right)^{2\alpha^{\mathrm{PS}}(t)}. \quad (19)$$

The residual factor g_0^2 is, in general, a function of t and should be determined by the comparison with experimental data. We use $(g^V_0)^2/4\pi = 0.796$ for the vector meson trajectory exchange, which is found from comparison with the available experimental data for K^{*0} production. We use this value for both the strangeness and charm production processes as we do not have any data for charm vector meson production. Since we are interested in identifying the major production mechanisms, we need to be able to distinguish between the pseudoscalar meson trajectory exchange and the vector meson trajectory exchange through measurable physical quantities. Because the pseudoscalar exchange mechanism is expected to be small, we consider two extreme cases, namely, vector-exchange dominance and pseudoscalar-exchange dominance. For this purpose, we adjust the value of g^{PS}_0 to achieve the condition that $d\sigma^{(\mathrm{PS})}/dt = d\sigma^{(\mathrm{V})}/dt$ at zero vector meson production angle, i.e., at $t = t_{\max}$. This leads to $(g^{\mathrm{PS}}_0)^2/4\pi = 1.1$ and 13.5 for the production of K^* and D^* mesons, respectively. Of course, the realistic case is between these two extreme cases, and the relative strength of the two mechanisms should be determined by experimental data.

The obtained differential cross sections for K^* and D^* production are exhibited in Figs. 3(a) and 3(b), respectively. Throughout the present study, the initial pion momentum in the laboratory frame is chosen to be $p_\pi = 6\,\mathrm{GeV}/c$ for strangeness production and 15 GeV/c for charm production. The V and PS Reggeon exchanges are shown by the solid and dashed curves, respectively, together with available experimental data of Ref. [26] for K^* production. Although the energy scale is different, it turns out that the cross section of charm production is suppressed compared with that of strangeness production, which is consistent with the observation made in Ref. [18]. One can see that both the vector-type Reggeon exchange and the pseudoscalar-type Reggeon exchange exhibit a similar t dependence in differential cross sections. This resemblance is clearly seen in the case of charm production, although the available data seem to prefer the vector-type exchange in the case of strangeness production. Therefore, the t dependence of cross sections cannot clearly distinguish the two exchanges. As we see in the next subsections, however, the situation changes for spin-density matrix elements and the angular distributions of $K^* \to K\pi$ and $D^* \to D\pi$ decay, where the difference between the two types of exchanges is revealed even at the qualitative level.

B. Spin-density matrix elements

The results for the spin-density matrix elements $\rho^0_{\lambda\lambda'}$ defined in Eq. (13) are presented in Fig. 4 for K^{*0} and D^{*-} production as functions of $(t_{\max} - t)$. We also limit our consideration to relatively small values of $|t|$ such that $|t_{\max} - t| \leqslant 2\mathrm{GeV}^2$, where the applicability of the QGSM can be justified. Shown in Fig. 4 are the results for the vector-type Reggeon exchange model and for the pseudoscalar-type Reggeon exchange

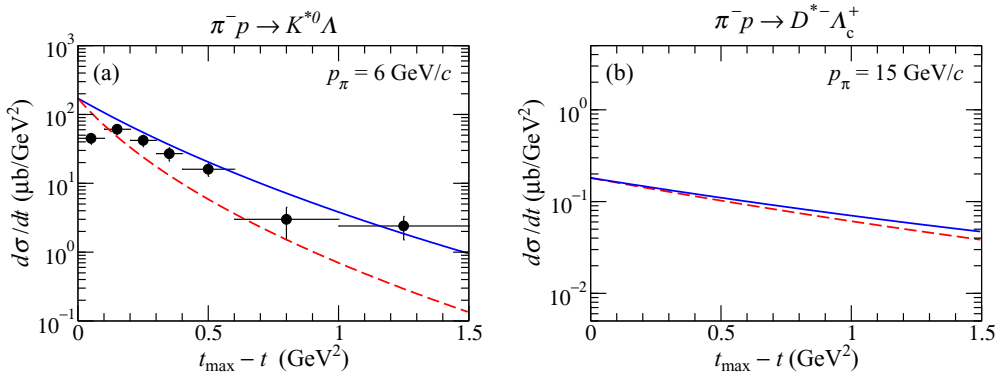

FIG. 3. Unpolarized differential cross sections of (a) $\pi^- + p \to K^{*0} + \Lambda$ and (b) $\pi^- + p \to D^{*-} + \Lambda_c^+$ for the vector (solid curves) and pseudoscalar (dashed curves) Reggeon exchanges. The experimental data for $\pi^- + p \to K^{*0} + \Lambda$ are from Ref. [26].

model, which are calculated in the s and t frames. Our results numerically confirm the symmetry properties, $\rho^0_{11} = \rho^0_{-1-1}$, $\rho^0_{\pm 10} = \rho^0_{0\pm 1}$, $\rho^0_{\pm 10} = -\rho^0_{0\mp 1}$, and $\rho^0_{1-1} = \rho^0_{-11}$.

In the case of vector-type Reggeon exchange, the matrix elements $\rho^0_{\lambda\lambda'}$ with $|\lambda| = |\lambda'| = 1$ are enhanced. This ascribes to the spin structure $\epsilon^{\mu\nu\alpha\beta} q_\mu p_{V\alpha} \varepsilon^*_\beta(\lambda_V)$ of the amplitude in Eq. (9). In the vector meson rest frame, where $p_V = (M_V, 0, 0, 0)$ and $\boldsymbol{q} = -\boldsymbol{p}_\pi$, this factor is proportional to the vector product of $\boldsymbol{\varepsilon}^*(\lambda_V) \times \boldsymbol{p}_\pi$. In the s frame and small-momentum transfers, $\boldsymbol{p}_\pi$ has a large z component and a small

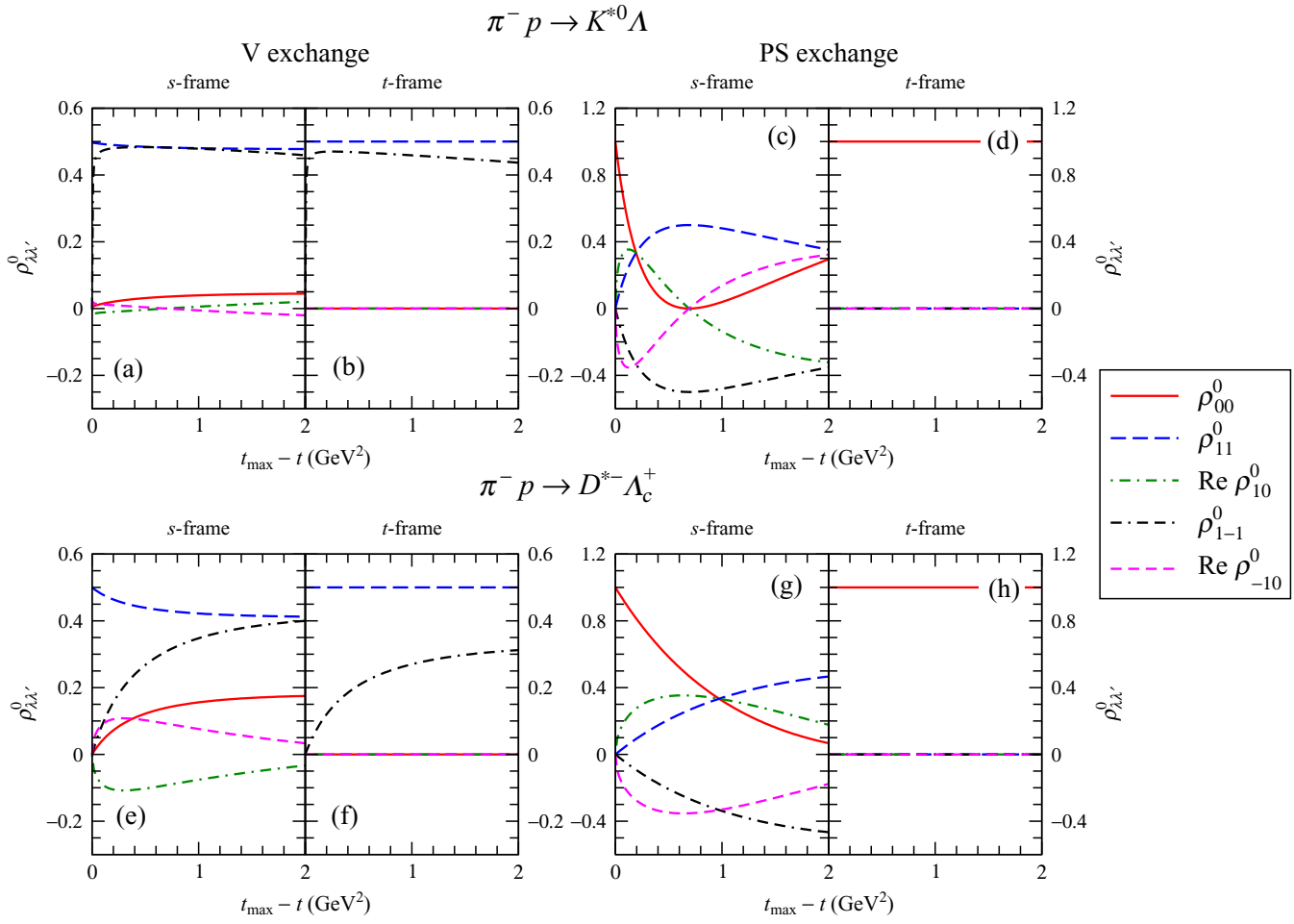

FIG. 4. The spin-density matrix elements $\rho^0_{\lambda\lambda'}$ defined in Eq. (13) as functions of $(t_{\max} - t)$ for K^{*-} production at $p_\pi = 6$ GeV/c [panels (a)–(d)] and for D^{*-} production at $p_\pi = 15$ GeV/c panels (e)–(h). The results for vector meson (V) and pseudoscalar (PS) Reggeon exchanges are in panels (a), (b), (e), and (f) and panels (c), (d), (g), and (h), respectively. The results in panels (a), (c), (e), and (g) were obtained in the s frame, while those in panels (b), (d), (f), and (h) were obtained in the t frame.

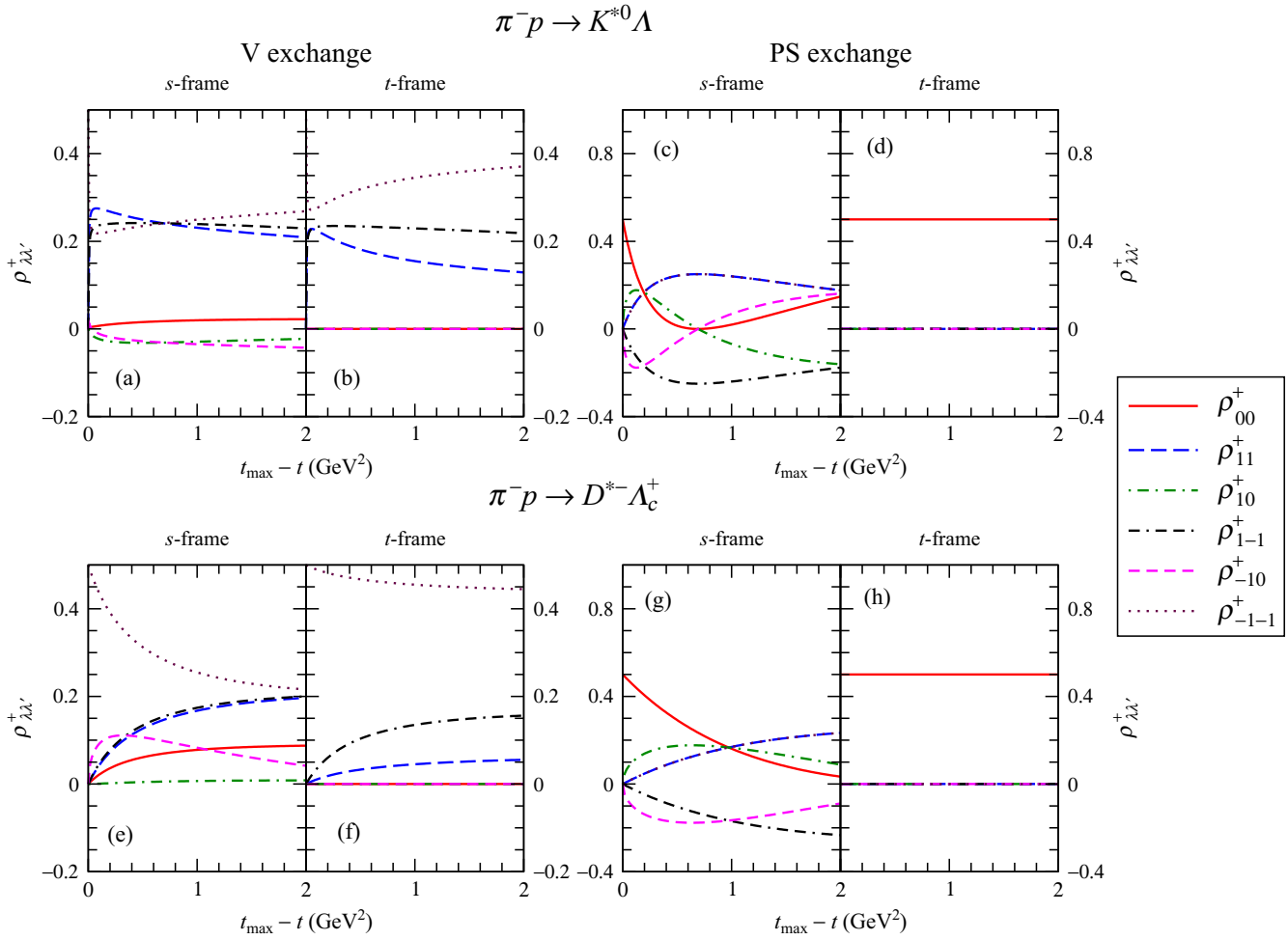

FIG. 5. The same as in Fig. 4 but for $\rho^+_{\lambda\lambda'}$.

x component, which leads to $\boldsymbol{\varepsilon}^*(\lambda_V) \times \boldsymbol{p}_\pi \simeq i\lambda_V \boldsymbol{\varepsilon}^*(\lambda_V)|\boldsymbol{p}_\pi|$ and thus causes the large enhancement of $\rho^0_{|\lambda|=1,\,|\lambda'|=1}$. In the t frame, $\boldsymbol{p}_\pi$ is parallel to the quantization axis, and this leads to $\rho^0_{\lambda\lambda'}$ with either $\lambda = 0$ or $\lambda' = 0$ vanishing. We also note that $\rho^0_{1-1} = 0$ at $t = t_{\rm max}$. This is because of the relation $\rho^0_{1-1} \propto \sin^2\theta$, where θ is the scattering angle of the vector

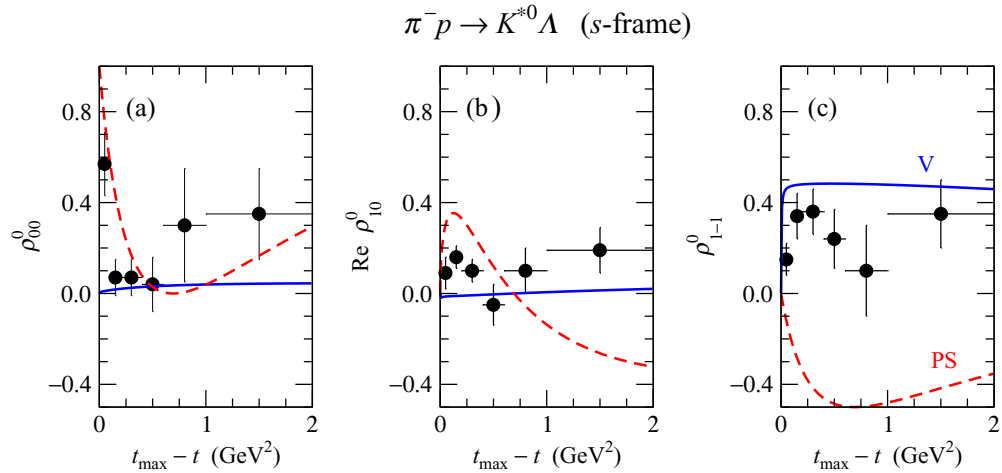

FIG. 6. Spin-density matrix elements for K^{*0} production in the s frame. Panels (a), (b), and (c) correspond to ρ^0_{00}, Reρ^0_{10}, and ρ^0_{1-1} matrix elements, respectively. The vector and pseudoscalar Reggeon exchange models are depicted by the solid and dashed curves, respectively. The experimental data are from Ref. [26].

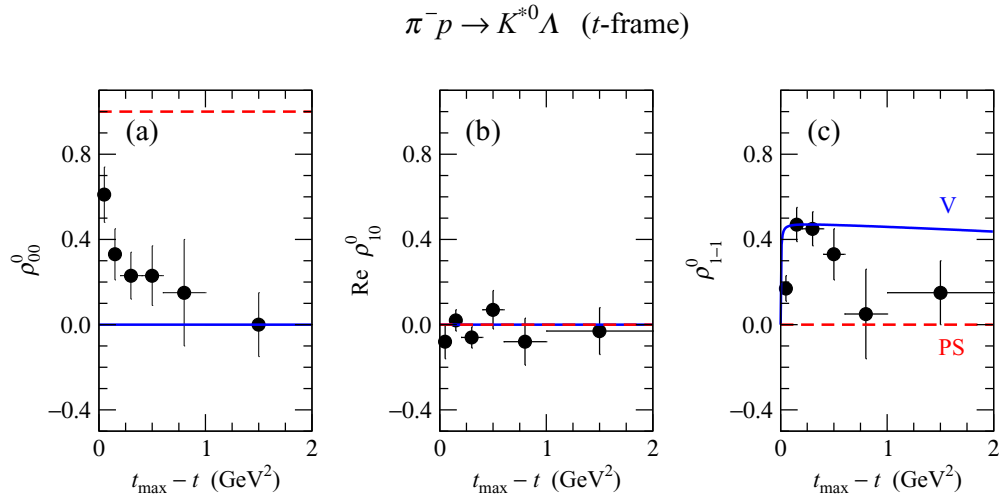

FIG. 7. The same as in Fig. 6 but in the t frame.

meson in the center-of-mass frame for the scattering process. All these observations hold also for the matrix element ρ^+_{1-1} as seen in Fig. 5.

In the case of pseudoscalar-type Reggeon exchange, however, the situation is quite different. The production amplitude of this mechanism is proportional to the scalar product, $\boldsymbol{\epsilon}^*(\lambda_V) \cdot \boldsymbol{p}_\pi$, which leads to a strong enhancement of ρ^0_{00} in the t frame, so that $\rho^0_{00} = 1$ and all the other $\rho^0_{\lambda\lambda'}$ vanish.

Shown in Fig. 5 are the results for $\rho^+_{\lambda\lambda'}$ defined in Eq. (14). In this case, the spin alignment of the outgoing hyperon is fixed to be $m_f = +\frac{1}{2}$. The absolute values of $\rho^\pm$ are smaller than

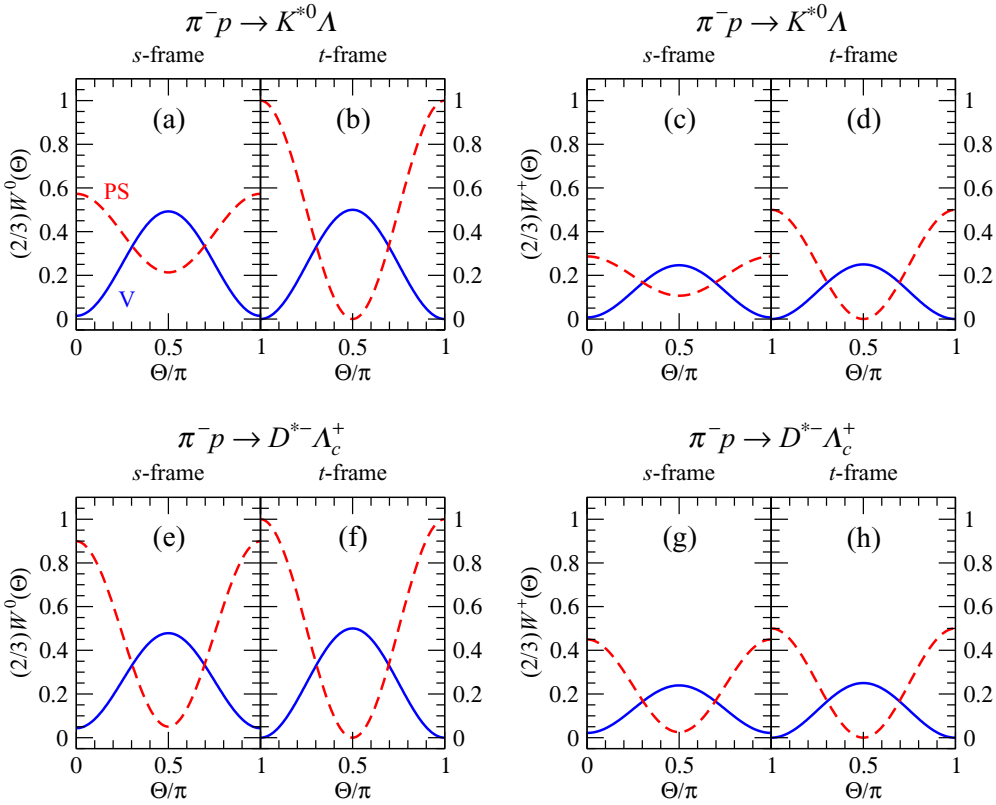

FIG. 8. Angular distributions $\frac{2}{3}\,W(\Theta)$ of Eq. (20) for K^* and D^* excitations are shown in the upper and lower panels, respectively. Panels (a), (b), (e), and (f) are for $\frac{2}{3}\,W^0(\Theta)$ and panels (c), (d), (g), and (h) are for $\frac{2}{3}\,W^+(\Theta)$. The results are given in both the s and t frames. The vector and pseudoscalar Reggeon exchange cases are depicted by the solid and dashed curves, respectively. Calculation is done for $|t_{\max} - t| = 0.1$ GeV^2 at $p_\pi = 6$ GeV/c for K^* production and $p = 15$ GeV/c for D^* production.

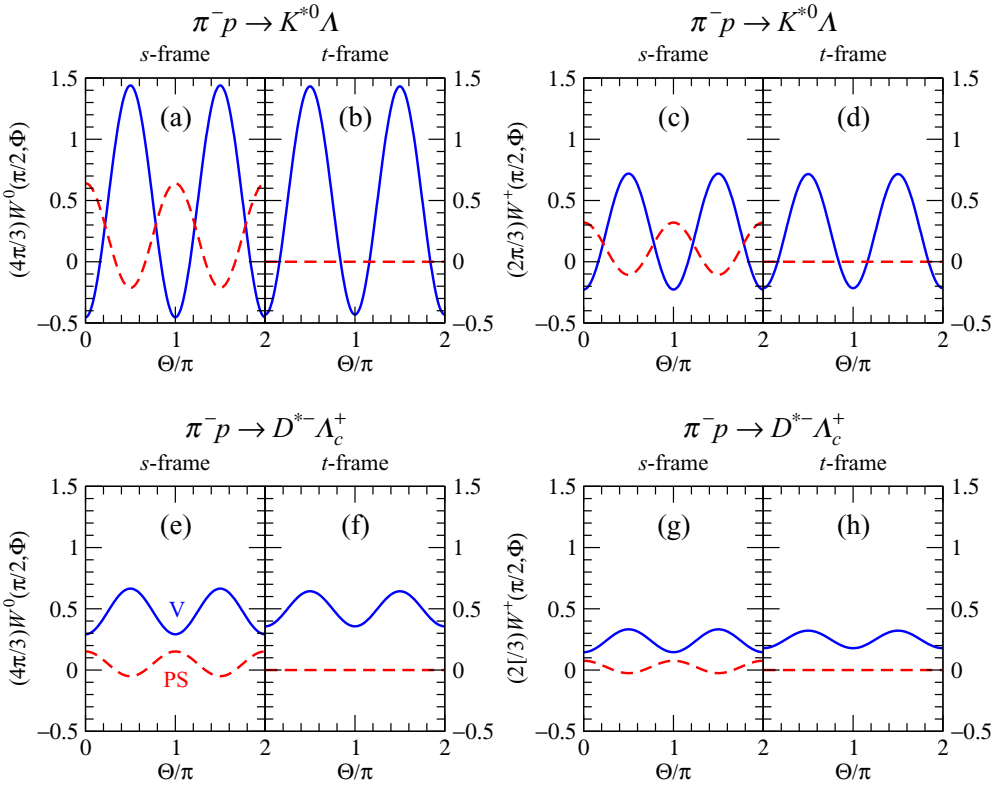

FIG. 9. The same as in Fig. 8 but for the azimuthal angle distributions $\frac{4\pi}{3}\,W(\Theta=\pi/2,\Phi)$ of Eq. (21).

those of ρ^0 by about a factor of 2 because of the difference in the numerators in Eqs. (13) and (14). The spin-density matrix elements $\rho^-_{\lambda\lambda'}$ can be obtained from $\rho^+_{\lambda\lambda'}$ using the following symmetry relations [27]: $\rho^-_{11}=\rho^+_{-1-1}$, $\rho^-_{00}=\rho^+_{00}$, $\rho^-_{-11}=\rho^+_{-11}$, $\rho^-_{10}=-\rho^+_{0-1}$, and so on.

In Figs. 6 and 7, we compare our results with the available experimental data of Ref. [26] for K^{*0} production in the s and t frames, respectively. Although the vector-exchange mechanism leads to a better agreement with the data than the pseudoscalar-exchange model, we can see that the vector-exchange model alone cannot successfully explain the data.[3] New experimental data for K^* production with higher precision are, therefore, strongly desired. In D^* production, the difference is also large enough to be verified by experiments and the analyses can be done at current or future experimental facilities.

C. Angular distributions of vector meson decays

The polar angle distributions of outgoing K and D mesons are obtained by integrating $W(\Theta,\Phi)$ of Eqs. (15) and (16) over the azimuthal angle Φ, which gives

$$\begin{aligned}\tfrac{2}{3}\,W^0(\Theta) &= \rho^0_{00}\cos^2\Theta + \rho^0_{11}\sin^2\Theta,\\ \tfrac{2}{3}\,W^\pm(\Theta) &= \rho^\pm_{00}\cos^2\Theta + \tfrac{1}{2}(\rho^\pm_{11}+\rho^\pm_{-1-1})\sin^2\Theta.\end{aligned}\quad (20)$$

These distributions are presented in Fig. 8 for the production and decays of K^* and D^* mesons at $|t_{\rm max}-t|=0.1$ GeV^2 with $p_\pi=6$ and 15 GeV/c, respectively.

In all cases, one can observe maxima at $\Theta=\frac{\pi}{2}$ for the vector trajectory exchange while minima are observed at the same angle for the pseudoscalar trajectory exchange. In other words, the distribution functions for the vector trajectory exchange display a cosine function shape, while those of the pseudoscalar trajectory exchange show a sine function shape. This is a direct consequence of the spin-density matrix elements ρ^0_{00} and ρ^0_{11} shown in Figs. 4 and 5.

The azimuthal angle distributions at a fixed polar angle Θ can also be obtained from Eqs. (15) and (16). At $\Theta=\frac{\pi}{2}$, we have

$$\begin{aligned}\frac{4\pi}{3}W^0\Big(\Theta=\frac{\pi}{2},\Phi\Big) &= \rho^0_{11}-\rho^0_{1-1}\cos 2\Phi,\\ \frac{4\pi}{3}W^\pm\Big(\Theta=\frac{\pi}{2},\Phi\Big) &= \frac{1}{2}(\rho^\pm_{11}+\rho^\pm_{-1-1})-\rho^\pm_{1-1}\cos 2\Phi.\end{aligned}\quad (21)$$

The corresponding distributions are shown in Fig. 9 at $|t_{\rm max}-t|=0.1$ GeV^2. In the s frame, the matrix element ρ^0_{1-1} takes a positive value for vector-type exchange and a negative value for pseudoscalar-type exchange. This difference means that $W(\frac{\pi}{2},\Phi)$ of vector-type exchange and pseudoscalar-type exchange are out of phase. The amplitudes of the oscillations in W^0 are found to be larger than those of $W^\pm$, which reflects the differences in ρ^0_{1-1} as shown in Figs. 4 and 5. For the pseudoscalar-Reggeon exchange in the t frame, $\rho^{0,+}_{\lambda,\lambda'}=0$ for

[3]We could confirm this conclusion through the comparison with the data obtained at $p_\pi=4.5$ GeV/c [26] as well.

$|\lambda| = |\lambda'| = 1$, and, therefore, the corresponding distributions $W(\frac{\pi}{2}, \Phi)$ vanish identically.

IV. SUMMARY AND CONCLUSION

In summary, we investigated the reactions of open strangeness K^* and open charm D^* vector mesons in πN scattering based on the quark-gluon string model. We found that unpolarized cross sections of K^* meson production are satisfactorily described by the QGSM with vector trajectory exchange. Although the contribution from pseudoscalar trajectory exchange is expected to be small, it also gives a similar t dependence of differential cross sections as the vector-type exchange model. Therefore, differential cross sections cannot be used to disentangle the two production mechanisms.

To verify the mechanisms of vector meson production, we then studied the angular distributions of vector meson decays. Unlike the cross sections, the spin-density matrix elements are sensitive to the spin structure of the production amplitude and, as a result, they show very different t-dependence and can be used to distinguish the vector and pseudoscalar exchanges. Furthermore, the density distribution functions are found to have completely different angle-dependence depending on the production mechanisms and can be used to probe the spin structure of the reaction amplitudes. In fact, the available data for spin-density matrix elements of K^* production show that the major production mechanism would be the vector-type exchange but it requires noticeable contributions from the pseudoscalar-type exchange. Because of the limited experimental data, we cannot estimate the relative strength between the vector and pseudoscalar exchanges, and, therefore, new data are strongly called for to investigate strangeness and charm production mechanisms.

We also presented our predictions for charm production. In this case, the t dependencies of differential cross sections of the vector and pseudoscalar exchanges are even closer to each other because of the similarity in the slope of vector and pseudoscalar trajectories, and thus the measurements of differential cross sections do not help pin down the production mechanisms. However, spin-density matrix elements and decay angular distributions are very sensitive to the production mechanisms as in the case of K^* production, and more detailed studies on these quantities are expected to shed light on our understanding of the strong interaction. In particular, the measurements for K^* and D^* productions are complementary to each other and are important to understand the dependence of the production mechanisms on the quark mass scale. All these predictions can be tested and verified in future experimental programs with pion beams, for instance, at the J-PARC facility.

ACKNOWLEDGMENTS

A.I.T. thanks the Asia Pacific Center for Theoretical Physics (APCTP) for kind hospitality given to him during his visit, which initiated this work. The work of Y.O. was supported by the Kyungpook National University Research Fund, 2015.

[1] Y. Morino, T. Nakano, H. Noumi, K. Shirotori, Y. Sugaya, T. Yamaga, K. Ozawa, T. Ishikawa, Y. Miyachi, and K. Tanida, Charmed baryon spectroscopy via the (π, D^{*-}) reaction, Proposal for Nuclear and Particle Physics Experiments at J-PARC (2012) [KEK/J-PARC-PAC 2012-19].

[2] V. Friese, The CBM experiment at GSI/FAIR, Nucl. Phys. A **774**, 377 (2006).

[3] Japan Proton Accelerator Research Complex, http://j-parc.jp/index-e.html.

[4] Facility for Antiproton and Ion Research in Europe GmbH, http://www.fair-center.eu.

[5] E. S. Swanson, The new heavy mesons: A status report, Phys. Rep. **429**, 243 (2006).

[6] N. Brambilla *et al.*, Heavy quarkonium: Progress, puzzles, and opportunities, Eur. Phys. J. C **71**, 1534 (2011).

[7] P. Nason, S. Dawson, and R. K. Ellis, The one particle inclusive differential cross section for heavy quark production in hadronic collisions, Nucl. Phys. B **327**, 49 (1989); **335**, 260(E) (1990).

[8] R. Vogt, The total charm cross section, Eur. Phys. J.: Spec. Top. **155**, 213 (2008).

[9] T. Kneesch, B. A. Kniehl, G. Kramer, and I. Schienbein, Charmed-meson fragmentation functions with finite-mass corrections, Nucl. Phys. B **799**, 34 (2008).

[10] E. G. de Oliveira, A. D. Martin, and M. G. Ryskin, Scale dependence of open $c\bar{c}$ and $b\bar{b}$ production in the low x region, Eur. Phys. J. C **77**, 182 (2017).

[11] A. B. Kaĭdalov, Electromagnetic form factors of hadrons at large Q^2 and the confinement effects, Pis'ma Zh. Eksp. Teor. Fiz. **32**, 494 (1980) [JETP Lett. **32**, 474 (1980)].

[12] A. B. Kaidalov, Hadronic mass-relations from topological expansion and string model, Z. Phys. C **12**, 63 (1982).

[13] A. B. Kaidalov and O. I. Piskunova, Production of charmed particles in the quark-gluon string model, Yad. Fiz. **43**, 1545 (1986) [Sov. J. Nucl. Phys. **43**, 994 (1986)].

[14] A. B. Kaidalov and P. E. Volkovitsky, Binary reactions in $\bar{p}p$ collisions at intermediate energies, Z. Phys. C **63**, 517 (1994).

[15] A. I. Titov and B. Kämpfer, Exclusive charm production in $\bar{p}p$ collisions at $\sqrt{s} \lesssim 15$ GeV, Phys. Rev. C **78**, 025201 (2008).

[16] A. Khodjamirian, Ch. Klein, Th. Mannel, and Y.-M. Wang, How much charm can PANDA produce?, Eur. Phys. J. A **48**, 31 (2012).

[17] K. G. Boreskov and A. B. Kaidalov, Production of charmed baryons in hadron-hadron collisions, Yad. Fiz. **37**, 174 (1983) [Sov. J. Nucl. Phys. **37**, 100 (1983)].

[18] S.-H. Kim, A. Hosaka, H.-C. Kim, and H. Noumi, Production of strange and charmed baryons in pion induced reactions, Phys. Rev. D **92**, 094021 (2015).

[19] S.-H. Kim, H.-C. Kim, and A. Hosaka, $K^0\Lambda$ and $D^-\Lambda_c^+$ production induced by pion beams off the nucleon, Phys. Rev. D **94**, 094025 (2016).

[20] C. Patrignani *et al.* (Particle Data Group), Review of particle physics, Chin. Phys. C **40**, 100001 (2016).

[21] L. Burakovsky, T. Goldman, and L. P. Horwitz, New quadratic baryon mass relations, Phys. Rev. D **56**, 7124 (1997).

[22] M. M. Brisudová, L. Burakovsky, and T. Goldman, Effective functional form of Regge trajectories, Phys. Rev. D **61**, 054013 (2000).

[23] V. G. J. Stoks and Th. A. Rijken, Soft-core baryon-baryon potentials for the complete baryon octet, Phys. Rev. C **59**, 3009 (1999).

[24] Th. A. Rijken, V. G. J. Stoks, and Y. Yamamoto, Soft-core hyperon-nucleon potentials, Phys. Rev. C **59**, 21 (1999).

[25] H. Becker *et al.* (CERN-MPI Munich Collaboration), Measurement of the reactions $\bar{p}p \to \bar{\Lambda}\Lambda$, $\bar{p}p \to \bar{\Lambda}\Sigma^0$ and $\bar{p}p \to \bar{\Lambda}$(missing mass) at 6 GeV, Nucl. Phys. B **141**, 48 (1978).

[26] D. J. Crennell, H. A. Gordon, K.-W. Lai, and J. M. Scarr, Two-body strange-particle final states in $\pi^- p$ interactions at 4.5 and 6 GeV/c, Phys. Rev. D **6**, 1220 (1972).

[27] K. Schilling, P. Seyboth, and G. Wolf, On the analysis of vector-meson production by polarized photons, Nucl. Phys. B **15**, 397 (1970); **18**, 332(E) (1970).